Geophysical Research Letters

Supporting Information for

Body Waves Retrieved from Noise Cross-correlation Reveal Lower Mantle Scatterers beneath the Northwest Pacific Subduction Zone

Limeng Zhang[123], Juan Li[123], Tao Wang[4], Fan Yang[123], Qi-Fu Chen[123]

[1]Key Laboratory of Earth and Planetary Physics, Institute of Geology and Geophysics, Chinese Academy of Sciences, Beijing, China

[2]Innovation Academy for Earth Science, Chinese Academy of Sciences, Beijing, China

[3]College of Earth and Planetary Sciences, University of Chinese Academy of Sciences, Beijing, China

[4]School of Earth Sciences and Engineering, Nanjing University, Nanjing, China

Contents of this file

Introduction

Figure S1 shows the comparison of observation data and synthetic seismograms. Figure S2 shows how to estimate the thickness and shear wave speed of the anomaly using waveform analysis. Figure S3 shows the waveform modeling to match P-to-P phase reflected off the scatterers and the analysis of the amplitude difference by different models. Figures S4-S6 show evidence of reflection waves in vespagram and the stability of the phases by bootstrapping. Figure S7 is used to demonstrate that a similar P410P phase is not affected by taper or surface coda. Figure S8 illuminates the complex structure in our study region.

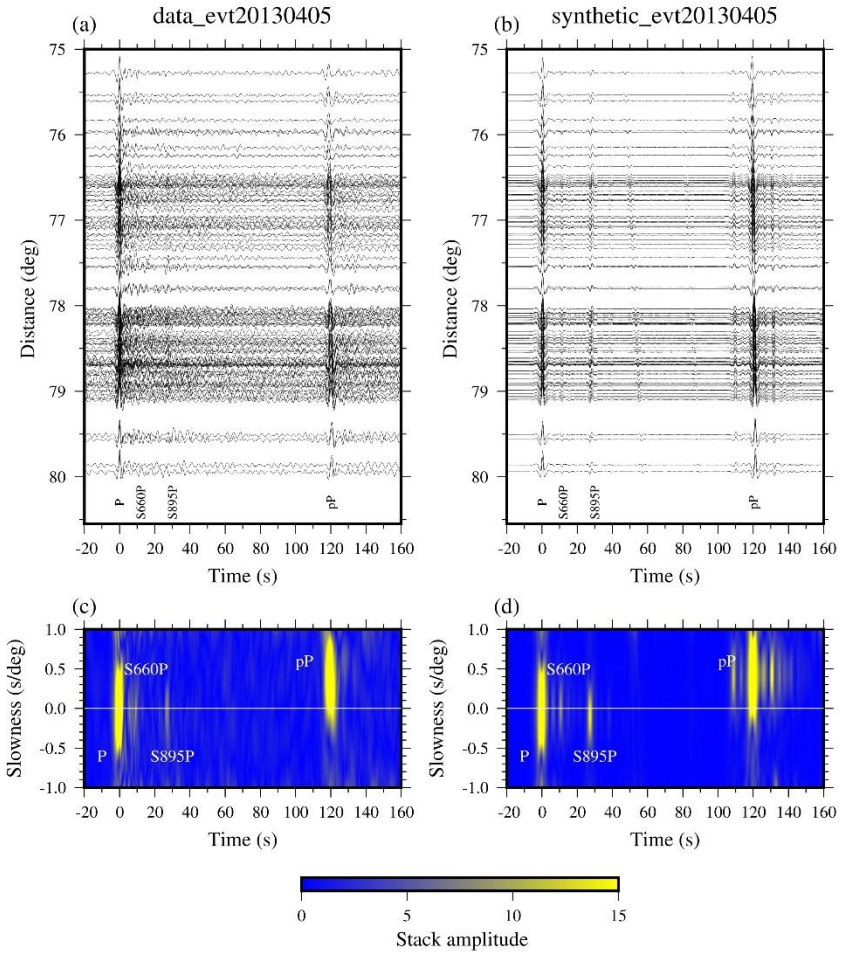

Figure S1. (a) The seismic record section and (c) Radon transform vespagram for event 20130405. (b) The corresponding synthetic seismograms calculated by the modified IASP91 model with a low-velocity layer with a thickness of 10 km located at 895 km and (d) its vespagram.

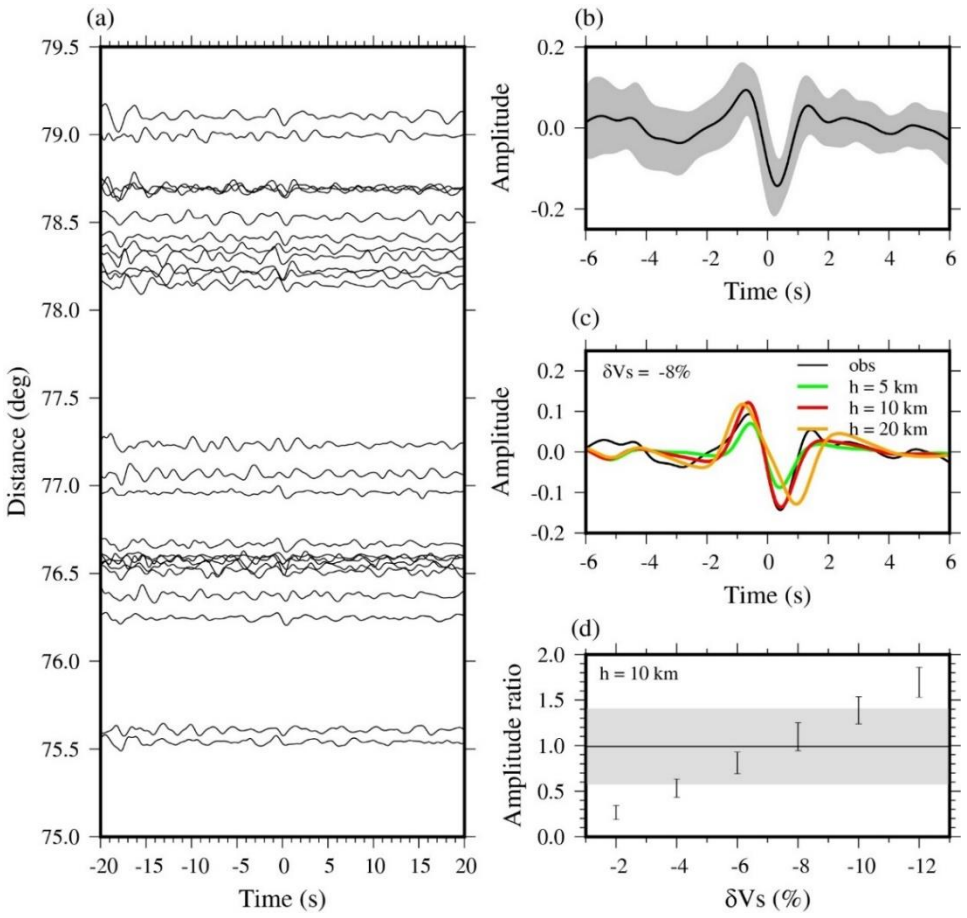

Figure S2. (a) The 26 selected traces with direct P-wave signal-to-noise ratios greater than 15 are shown in the section and aligned with the SdP phase (at time 0). The amplitude was normalized according to the direct P-wave. We calculated the standard deviation of the signal in the time window 30–40 s after the direct P-wave; this is defined as the noise level. (b) The black line shows the summation of the waveforms in panel (a), and the gray envelope indicates the standard deviation range of the data. (c) Synthetic seismograms were calculated for models with different thicknesses of the low Vs layer to fit the observed SxP phase (the black line in panel (b)). Thicker layers show broader phase pulses. The case of δVs = −8% is shown. (d) The amplitude ratio, defined by the maximum amplitude of the SxP phase relative to that of the S660P phase varies with δVs. The amplitude ratio of the observation in panel (b) is 0.99, and a line is marked through it. Synthetic seismograms for models with different Vs values but a fixed thickness of 10 km was calculated, and the value of the amplitude ratio was obtained for an epicentral distance of 75–80°. The vertical bars show the maximum and minimum values of the amplitude ratio.

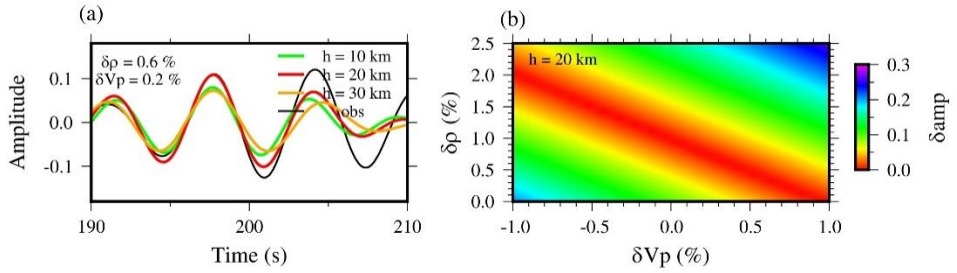

Figure S3. (a) Synthetic seismograms were calculated for the P-to-P phase for different thicknesses of the velocity anomaly. The curves shown here are for models with δρ = 0.6%, δVp = 0.2%, and δVs = −7.2%, which are constrained by the teleseismic SdP phases analyzed in our study. The velocity structure, especially around the MTZ, is adjusted first to match the observed P410P and P660P phases; a thick transitional 660-km discontinuity is required. The amplitude of the P-to-P phase is primarily determined by the δVp and δρ values. (b) The trade-off between δVp and δρ. A linear change in δVp and δρ will generate a reasonably good fit to the observations. Here, we show the variation in the maximum amplitude difference in the P-to-P phase between the observations and the synthetic values (δamp) calculated for different δVp or δρ values when the thickness is fixed to 20 km.

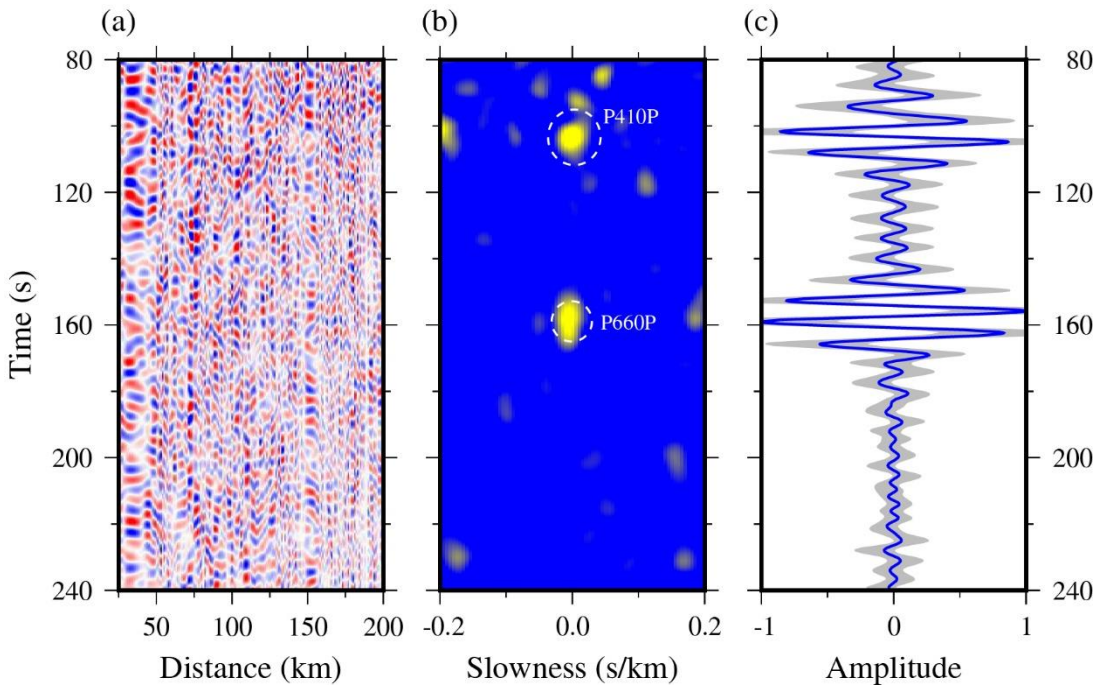

Figure S4. (a) The normal move-out corrected curves with mid-points located within region I are shown, sorted by distance. (b) Vespagram of all traces in (a) calculated by a Radon transformation. The slowness of clustered energies arriving at ~100 s and ~160 s is both around zero, which indicates the phases are reflected waves. (c) The stacked curves calculated via a phase weighted stacking scheme for the traces in panel (a). The grey area is the 95 % confidence interval by bootstrapping.

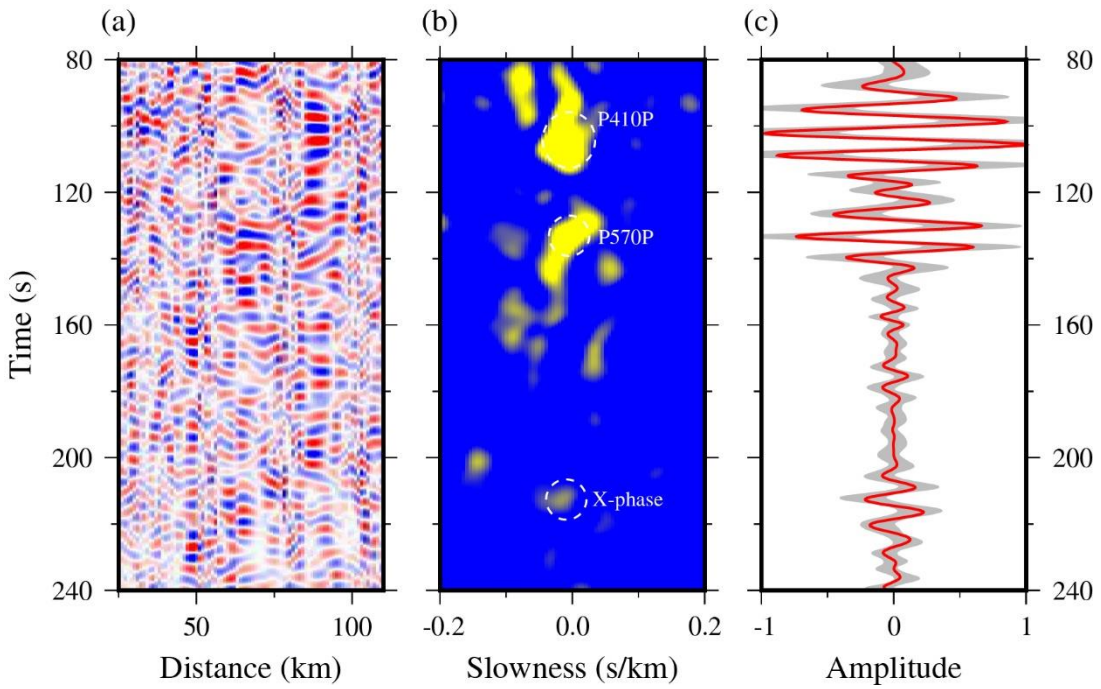

Figure S5. (a) The normal move-out corrected curves with mid-points located within region II are shown, sorted by distance. (b) Vespagram of all traces in (a) calculated by a Radon transformation. The slowness of clustered energies corresponding to seismic phases at ~100 s and ~130 s is around zero, which indicates the phases are reflected waves. The scheme of stacking enhanced weak but coherent signals. (c) The stacked curves calculated via a phase weighted stacking scheme for the traces in panel (a). The grey area is the 95 % confidence interval by bootstrapping. The stacked curve lies within the confidence interval, which indicates that the X-phase at ~218 s is stable.

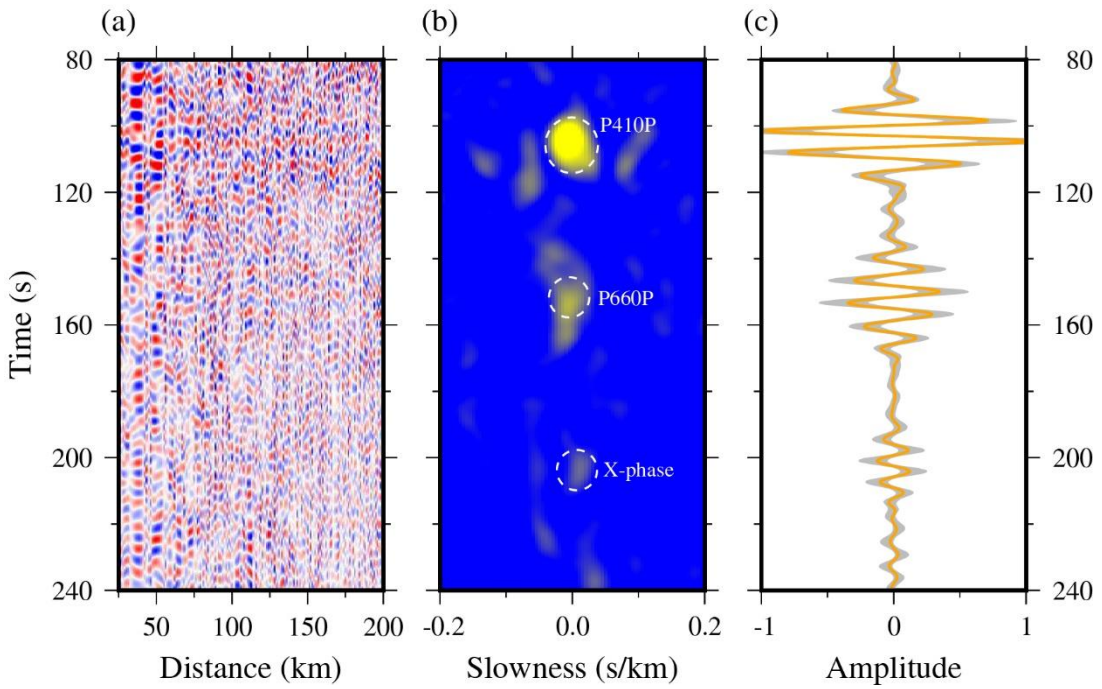

Figure S6. (a) The normal move-out corrected curves with mid-points located within region III are shown, sorted by distance. (b) Vespagram of all traces in (a) calculated by a Radon transformation. The slowness of clustered energies corresponding to seismic phases is concentrated near zero, which indicates the phases are reflected waves. (c) The stacked curves calculated via a phase weighted stacking scheme for the traces in panel (a). The grey area is the 95 % confidence interval by bootstrapping. The stacked curve lies within the confidence interval, which indicates that the X-phase at ~200 s is stable.

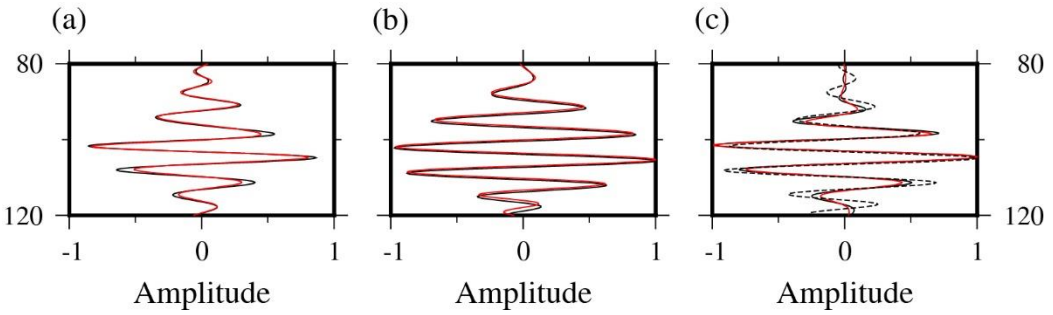

Figure S7. (a) The black line shows the P410P phase without tapering in region I. The red line is the P410P with tapering. (b) the same as (a) in region II. (c) the same as (a) in region III. In addition, the dashed line indicates the stacked result with distances of station-pairs less than 100 km in region III. The results are almost the same with or without taper. The travel time of surface wave is much smaller than that of the P410P at a distance smaller than 100 km, and the surface coda won't affect the body phases arrived later. We also get almost the same phase by stacking cross-correlations with different distances, which shows the stability of P410P phase in region III.

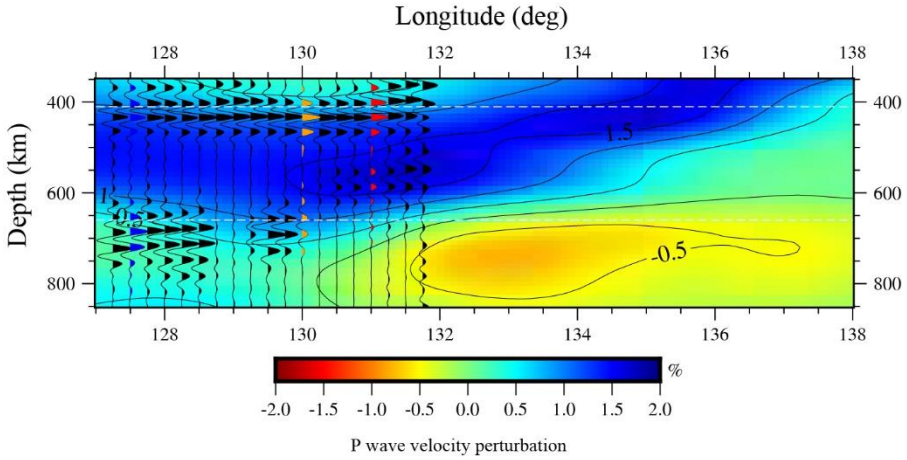

Figure S8. The cross-correlation curves along the latitude 43.5 °N is plotted with the seismic velocity map added as the background (Fukao and Obayashi, 2013). The time-depth transformation of the correlation is based on the iasp91 model. The center of three regions are (43.5°N, 127.5°E), (43°N, 131°E), and (43.75°N, 130°E), respectively. The blue, red and orange traces represent the retrieved body waves in three corresponding regions. The velocity structure beneath region II is complicated which might result in the spatial variation of the observed P660P.